

Journal of Materials Chemistry A

Accepted Manuscript



This is an *Accepted Manuscript*, which has been through the Royal Society of Chemistry peer review process and has been accepted for publication.

Accepted Manuscripts are published online shortly after acceptance, before technical editing, formatting and proof reading. Using this free service, authors can make their results available to the community, in citable form, before we publish the edited article. We will replace this *Accepted Manuscript* with the edited and formatted *Advance Article* as soon as it is available.

You can find more information about *Accepted Manuscripts* in the [Information for Authors](#).

Please note that technical editing may introduce minor changes to the text and/or graphics, which may alter content. The journal's standard [Terms & Conditions](#) and the [Ethical guidelines](#) still apply. In no event shall the Royal Society of Chemistry be held responsible for any errors or omissions in this *Accepted Manuscript* or any consequences arising from the use of any information it contains.

The Effect of Soft Nanoparticles Morphologies on Thin Film Composite Membrane Performance

Qiang Fu,^{ab} Edgar H. H. Wong,^b Jinguik Kim,^{ab} Joel M. P. Scofield,^{ab} Paul A. Gurr,^{ab}
Sandra E. Kentish^a and Greg G. Qiao^{*ab}

^a Cooperative Research Centre for Greenhouse Gas Technologies, Department of Chemical and Biomolecular Engineering, The University of Melbourne, Parkville, VIC 3010, Australia.

^b Polymer Science Group, Department of Chemical and Biomolecular Engineering, The University of Melbourne, Parkville, VIC 3010, Australia.

* Corresponding author. Tel: +61 3 8344 8665; Fax: +61 3 8344 4153.

E-mail address: gregghq@unimelb.edu.au (G. G. Qiao)

Abstract: Well-defined branched and densely cross-linked soft nanoparticles (SNPs) were synthesized and incorporated into a poly(ether-*b*-amide) (Pebax[®]) matrix to form the selective layer of thin film composite (TFC) membranes. The fabricated TFC membranes exhibited distinct gas separation abilities. These results reveal the effect of SNPs morphologies on the membrane performance. This study may provide insights and novel strategies to fabricate highly permeable membrane materials for carbon dioxide (CO₂) capture.

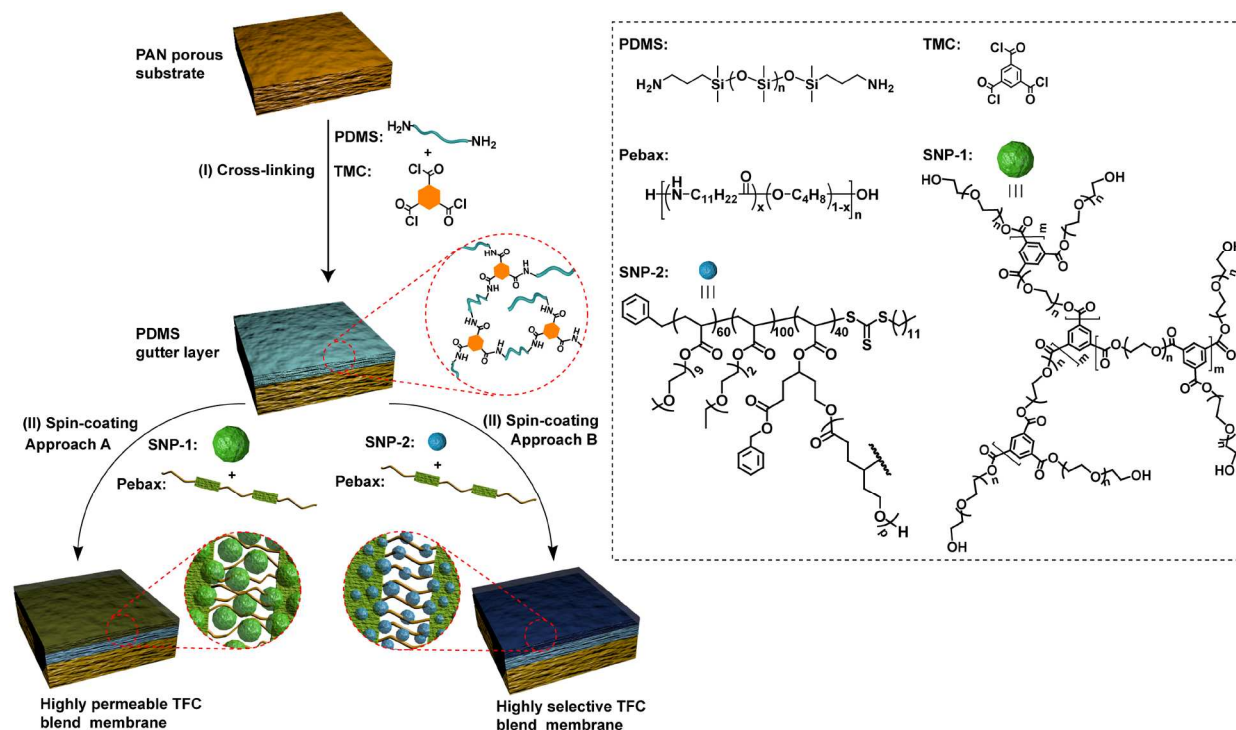
Currently, a significant world-wide effort is being directed towards technologies that will reduce CO₂ emissions into the atmosphere.¹ The use of polymeric membranes has the potential to substantially reduce the energy required to capture CO₂ for geo-sequestration or industrial re-use while having a smaller environmental and physical footprint than existing solvent systems.^{2,3} However, current dense film membranes are in many cases not competitive for large scale applications due to their low CO₂ permeance (flux).⁴ For example, state-of-the-art membranes exhibit a CO₂ permeance of about 110 GPU (1 GPU = 10⁻⁶ cm³(STP) cm⁻² s⁻¹ cmHg⁻¹).⁵ Recently, the development of thin film composite (TFC) membranes has attracted much attention.⁶⁻¹² This class of membrane is typically composed of a porous support coated with a highly permeable gutter layer, which is in turn coated with a thin selective layer.¹³⁻¹⁵ The fabrication of the selective

layer as an ultrathin film (≤ 400 nm) is more commercially viable than dense film membranes, due to the increased flux and reduced consumption of expensive materials.

Improved polymeric materials with excellent gas separation performance can be obtained either by designing and synthesizing new polymers^{16, 17} or by modifying or blending existing commercial polymers with organic^{18, 19} or inorganic compounds.^{20, 21} Since the ethylene glycol (EG) unit can exhibit favorable interactions with CO₂ relative to other lighter gases,²² recent studies have focused on the incorporation of polyethylene glycol (PEG) additives into the existing membrane materials, i.e. poly(ether-*b*-amide) (Pebax[®]). Pebax[®] is a thermoplastic elastomer combining linear chains of rigid polyamide (PA) segments interspaced with flexible polyether (PE) segments. Lee and co-workers firstly reported the preparation of Pebax[®] series membranes for gas separation.^{23, 24} Car and Peinemann reported the fabrication of Pebax[®] 1657/PEO₂₀₀ blend membrane system.⁸ Similarly Yave *et. al.* reported the fabrication of poly(ethylene oxide)-poly(butylene terephthalate) (PEO-PBT)/PEO₂₀₀ selective layers, and they observed an increase in CO₂ permeability without loss of selectivity.¹⁸ However, the development of effective PEG additives has been limited to low molecular weight (MW) linear PEG oligomers (with *ca.* MW < 300 Da) as high molecular weight PEGs result in increased crystallinity, which leads to a decrease of permeability.²⁵ Recently, we have demonstrated the ability of a class of star-like soft nanoparticle (SNPs) to form localized, high flux, CO₂ permeable domains within the selective layer, which in turn leads to an increase in the gas separation performance compared to linear polymers.¹⁹ Here, we hypothesize that the incorporation of PEG-based amorphous SNPs with different morphologies and optimized proportions of ethylene glycol (EG) moieties into the thin selective layer can further improve the gas separation performance. These SNP additives were designed to comprise of (i) a PEG-based CO₂ permeable core, (ii) a shell which is compatible with the polymer matrix and (iii) a size significantly smaller than the thickness of the selective layer in order to avoid defects in the resulting TFC membranes.

In the present work, the two types of PEG-based amorphous SNPs with different morphologies (Scheme 1, Fig. S1 and Fig. S2) were synthesized. One is highly branched and the other is densely cross-linked nanoparticles. They were physically blended with Pebax[®] to afford the selective layers of the TFC membranes. The polymeric linear

precursor (LP) of SNP-2 was also blended with Pebax to provide direct comparison. The synthesized LP and SNPs were fully characterized by dynamic light scattering (DLS) and proton magnetic resonance spectroscopy (^1H NMR). The TFC membranes were fabricated and characterized by scanning electron microscopy (SEM), X-ray photoelectron spectroscopy (XPS) and X-ray diffraction (XRD) measurements. The effect of SNPs morphologies on gas separation performance was investigated.



Scheme 1. The fabrication of Pebax[®]/SNPs TFC membranes. Cross-linked PDMS gutter layer was prepared by spin coating mixtures of amino-terminated PDMS and TMC (Step I). Selective layers were fabricated by spin-coating mixtures of Pebax[®] 2533 and SNPs onto the cross-linked PDMS gutter layer (Step II).

A commercially available PAN microporous substrate was employed as a support to construct the TFC membrane. A solution of amino-terminated PDMS and trimesoyl chloride (TMC) was spin-coated onto the PAN substrate to afford a cross-linked and highly permeable gutter layer (Scheme 1, step I). This PDMS intermediate layer prevents the penetration of dilute polymer solution into the PAN structure as well as rendering the entire membrane surface smoother. Thereafter, the fabricated SNPs were blended into a Pebax[®] 2533 matrix and the mixture was spin-coated onto the PDMS gutter layer to form the selective layer with dispersed SNPs (Scheme 1, step II). Their ability to selectively

separate CO₂ from N₂ was tested by utilizing an in-house built constant pressure variable volume (CPVV) apparatus (Fig. S3).

The two types of SNPs are labeled as SNP-1 and SNP-2. SNP-1, a hyperbranched organic nanoparticle, was synthesized *via* condensation polymerization of PEG₄₀₀ ($M_n = 400$ Da) with TMC at room temperature (Fig. S1A). The PEG₄₀₀ segments provide flexibility and a high affinity for the polyether phase of Pebax ® leading to a homogeneous dispersion of the SNP-1 within the matrix. The hydrodynamic diameter (D_H) of SNP-1 was determined to be 47.3 nm by DLS measurements (Fig. 1A). The chemical structure of SNP-1 was further characterized by ¹H NMR spectroscopic analysis. The molar ratio of PEG₄₀₀ to TMC was calculated to be 0.93, by comparing the integral ratio of the PEG methylene protons (b , $\delta_H = 4.41$ - 4.51 ppm) adjacent to the ester group and TMC aromatic protons (a , $\delta_H = 8.80$ - 8.94 ppm) (Fig. S1B).

SNP-2 is a single-chain polymeric nanoparticle and it was generated by the intramolecular cross-linking of collapsed single polymer chains.²⁶ Specifically, a linear precursor (LP) composed of oligo(ethylene glycol) methyl ether acrylate, di(ethylene glycol) ethyl ether acrylate and 4-(acryloyloxy)- ϵ -caprolactone was made *via* reversible addition fragmentation chain transfer (RAFT) polymerization,²⁷ followed by ring-opening polymerization (ROP)²⁸ in the presence of a nucleophilic initiator (benzyl alcohol) and organo catalyst (methanesulfonic acid) to afford SNP-2 (Fig. S2). DLS analysis indicated that the formed soft nanoparticle (SNP-2) has a smaller mean hydrodynamic diameter (D_H) of 4.8 nm compared to 7.2 nm for its linear precursor LP (Fig. 1A). All other characterization data confirming the successful formation of SNP-2 are described in our previous publication.²⁶

It is well known that one drawback of using pure PEG in separation membranes is its strong tendency to crystallize.² However, using our previously reported strategy,⁹ both SNPs used in this work are amorphous, due to their highly cross-linked structures. The XRD patterns of SNP-1 and SNP-2 (Fig. 1B), both showed broad peaks around 22.0° confirming the suppression of PEG crystallinity.

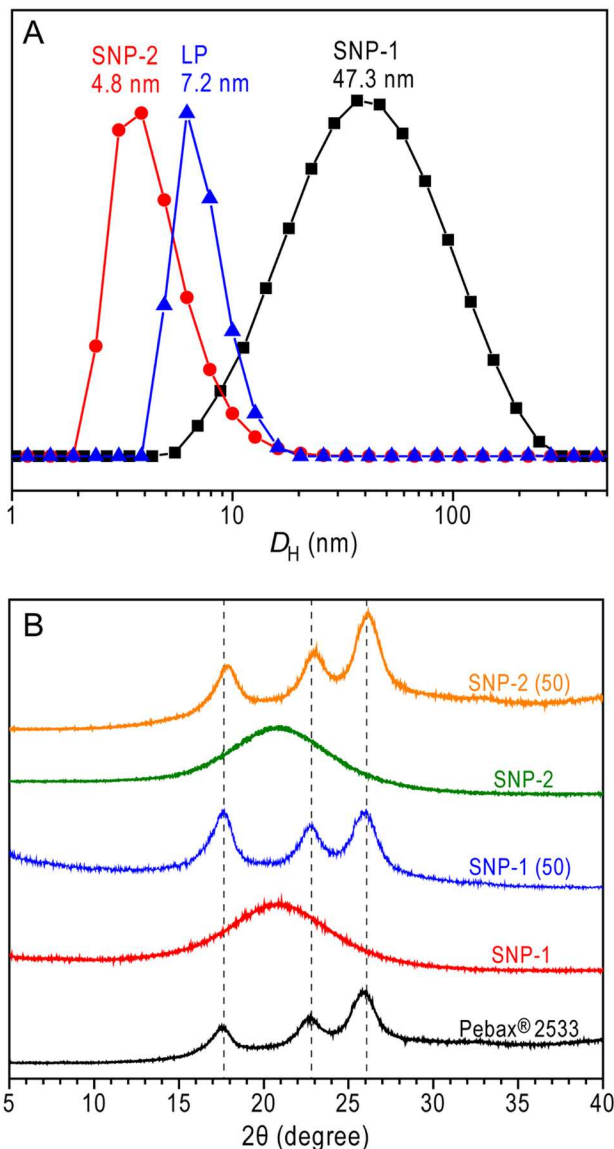


Fig. 1 (A) Volume-average hydrodynamic diameter distribution curves of SNP-1, SNP-2 and its linear precursor (LP). (B) X-ray diffraction diagrams of Pebax® 2533 TFC membrane, SNP-1, SNP-2 and their TFC membranes: SNP-1 (50) and SNP-2 (50).

The PDMS gutter layer was prepared by spin-coating the TMC and amino-terminated PDMS mixture onto a PAN substrate. The successful cross-linking of the amino groups was confirmed by XPS and ATR-FTIR analysis. High resolution XPS spectra of C 1s and O 1s (Fig. S4A-B) provide detailed information about the surface functional groups present on the PDMS gutter layer. Additionally, the ATR-FTIR spectrum of the cross-linked PDMS gutter layer is displayed in Fig. S5. The result indicates that polyamide has formed after spin-coating since the strong band at 1500 cm^{-1} , which is characteristic of N-H (amide ii), is present. In order to estimate the thickness of the PDMS layer, cross-

sectional SEM analysis was carried out on a number of different samples and an example is shown in Fig. 2A. The thickness of the PDMS skin layer is less than 200 nm. The gas transport properties of the PDMS gutter layer were tested by the apparatus shown in Fig. S3. The average CO₂ permeance reached up to 2500 ± 100 GPU and the CO₂/N₂ selectivity is approximately 9, which is in agreement with previously published data¹⁴ and demonstrates the successful formation of a PDMS gutter layer free of defects.

Noteworthy, during the formation of a linear polymer from acyl chloride and diamine, a base is commonly used to give a high molecular weight polyamide. However, in the formation of network PDMS gutter layer, we avoided the use of a base to reduce the reaction rate so that the gutter layer will have a longer shelf-life. Since we used TMC as a multi-functional cross-linker, a stable polymeric network was formed. This method also avoids the need for removing the urea by-products after membrane formation.

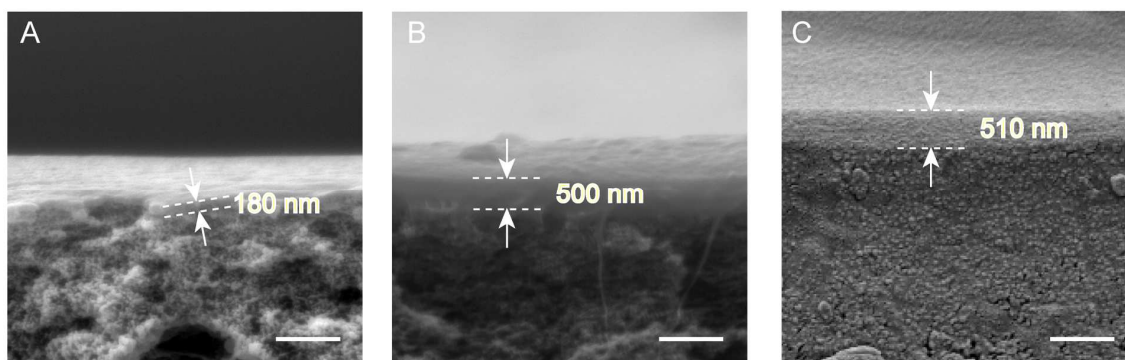


Fig. 2 SEM images of the cross-section of the TFC membranes showing (A) PDMS gutter layer, (B) PDMS gutter layer plus SNP-1 (50) and (C) SNP-2 (50) layers, respectively. The scale bar represents 1 μm.

The Pebax[®] 2533/SNPs blended selective layers were prepared by spin-coating respective polymer solutions onto PAN substrates which were pre-coated with the PDMS gutter layer. The XRD patterns obtained for Pebax[®] 2533 and Pebax[®] 2533/SNPs TFC membranes (Fig. 1B) showed three similar crystalline peaks, which are attributed to the crystallization of the polyamide ($2\theta = 22.9^\circ$) and polyether ($2\theta = 17.8$ and 26.0°) segments, indicating a homogenous dispersion of SNPs in the Pebax[®] matrix. The cross-sectional morphologies of the TFC membranes with 50 wt % SNPs content (SNP-1 (50) and SNP-2 (50)) observed by SEM analysis are illustrated in Fig. 2B and 2C, respectively. The thickness of the selective layers alone were estimated to be less than 330 nm in all cases (Table S1), by subtracting the thickness of the PDMS gutter layer from the

observed thickness of the combined selective and gutter layers. The chemical changes that occurred as a result of the coating of the selective layer on the PDMS gutter layer were further ascertained by XPS analysis. Fig. S4C-D shows the high resolution XPS spectra of SNP-1 (50). The C 1s and O 1s signals have been altered after coating with the selective layer. For example, the C 1s spectra signal at 286.6 eV is ascribed to the carbon ether bond C-O and the O 1s spectra signal at 534.0 eV is due to the oxygen in the O-C=O bond. Fig. S5 shows the ATR-FTIR spectra of the SNP-1 (50) and SNP-2 (50) composite membranes. The strong band at 1720 cm^{-1} assigned to C=O stretching vibration and the band around $2860\text{-}3100\text{ cm}^{-1}$ assigned to C-H stretching vibration are characteristics of carboxyl group due to the addition of SNPs. These results confirmed the preparation of Pebax[®] 2533/SNPs selective layers.

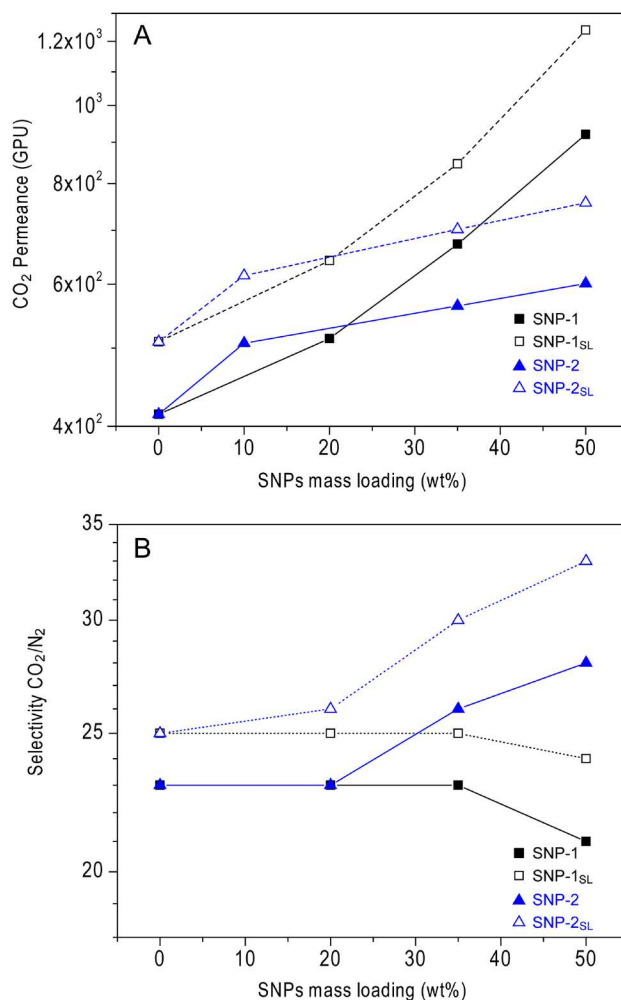


Fig. 3 (A) CO₂ permeance and (B) CO₂/N₂ selectivity of the TFC membranes as a function of SNPs mass fraction tested at 35 °C and 340 kPa.

The gas transport properties of the TFC membranes as a function of the SNP mass fraction (0-50 wt. %) have been measured at a temperature of 35 °C and a feed pressure of 340 kPa. As shown in Fig. 3A and Table S1, the CO₂ permeance of these TFC membranes increases with the increase in SNP-1 mass fraction. We hypothesize that the significant increase in gas permeance can be attributed to three separate effects. Firstly, the increase of SNP-1 mass fraction results in a higher overall concentration of EG moieties in the selective layer, which in turn increases the CO₂ solubility.²⁵ Secondly, the branched architecture of SNP-1 increases the fractional free volume (FFV) of the selective layer, which leads to an increase in CO₂ diffusivity. Thirdly, the homogenous dispersion of SNP-1 in the polyether phase can disrupt the chain packing and increase the inter-chain distance (*d*-space), which also leads to an increase in diffusivity (Scheme 1, Approach A). These three aspects make the dispersed SNP-1 perform as a major CO₂ transport pathway. The TFC membrane containing 50 wt. % of SNP-1 showed an increase in CO₂ permeance that is more than double the permeance of the unblended membrane (from 414 to 920 GPU, Table S1), while maintaining a CO₂/N₂ selectivity of *ca.* 21. However, the SNP-1 (60) TFC membrane with 60 wt. % SNP-1 showed lower CO₂/N₂ selectivity of *ca.* 16 with higher CO₂ permeance of 1,170 GPU (Table S1). This loss in selectivity results from the further increase in FFV, which causes the N₂ diffusivity to increase at a greater rate than CO₂. These results indicate that there is an optimal content of SNP to fabricate TFC membranes with desirable CO₂ separation performance.

When highly cross-linked SNP-2 was employed, the Pebax[®] 2533/SNP-2 TFC membranes exhibited an enhanced CO₂ permeance with a not compromised, but further increased CO₂/N₂ selectivity. For example, the CO₂ permeance for SNP-2 (50) increased from 414 to 600 GPU and the CO₂/N₂ selectivity increased from 23 to 28. This is rare but significant observation. We hypothesized that the increase of SNP-2 mass fraction results in a higher overall mean concentration of EG moieties, which leads to an increase in CO₂ solubility. However, the homogenous dispersion of SNP-2 nanoparticles only induce a smaller increase in FFV in the polyether phase due to its smaller particle size (4.8 nm) and collapsed architecture, compared to SNP-1 (Scheme 1, Approach B). The smaller particle size also results in a smaller increase in CO₂ diffusivity. Therefore, the Pebax[®]

2533/SNP-2 TFC membranes displayed a stronger increase in selectivity and a moderate increase in CO₂ permeance in comparison with their SNP-1 counterparts. The incorporation of both PEG-based SNPs into the Pebax[®] 2533 matrix enhanced their gas separation ability. These results also demonstrate that the SNPs' size and morphology play an important role in the TFC membrane performance. In addition, we have also prepared a LP (50) TFC membrane by blending 50 wt. % linear precursor of SNP-2 into the Pebax[®] 2533. This TFC membrane showed a lower CO₂/N₂ selectivity of *ca.* 15 and a much higher CO₂ permeance of 1,280 GPU, reflecting significant increases in FFV (Table S1).

Single gas measurements of the SNP-1 TFC membranes across a range of feed pressures at 35 °C were also investigated. Fig. S6 and Table S2 present the CO₂ permeance and CO₂/N₂ selectivity as a function of feed gas pressure. For Pebax[®] and SNP-1 (50) TFC membranes, the CO₂ permeances increased by *ca.* 80 and 100 GPU respectively, when the feed pressure was increased from 340 to 1,000 kPa. The CO₂/N₂ selectivity of Pebax[®] and SNP-1 (50) slightly decreased with increasing feed gas pressure. These results can be attributed to CO₂-induced plasticization.²⁹ Although plasticization occurred at these higher operational pressures, the CO₂/N₂ selectivity of the SNP-1 (50) TFC membrane still maintained a value of *ca.* 20 with a CO₂ permeance of greater than 1,000 GPU.

The calculation of permeability through the selective layer can be used to reveal the true potential of the membrane materials. Therefore, the permeance, permeability and selectivity of the selective layer were calculated using previously published methods.^{9, 19} As shown in Table S1, the CO₂ permeability of the selective layer increased from 158 to 397 Barrer with the addition of 50 wt% SNP-1 (denoted by SNP-1 (50)_{SL}) without the loss of selectivity. Moreover, the CO₂/N₂ selectivity increased from 25 to 33 for the SNP-2 (50) with a CO₂ permeability of 250 Barrer. This concurrent increase in CO₂ permeability and CO₂/N₂ selectivity presents a new direction for the development of next generation gas separation membranes.

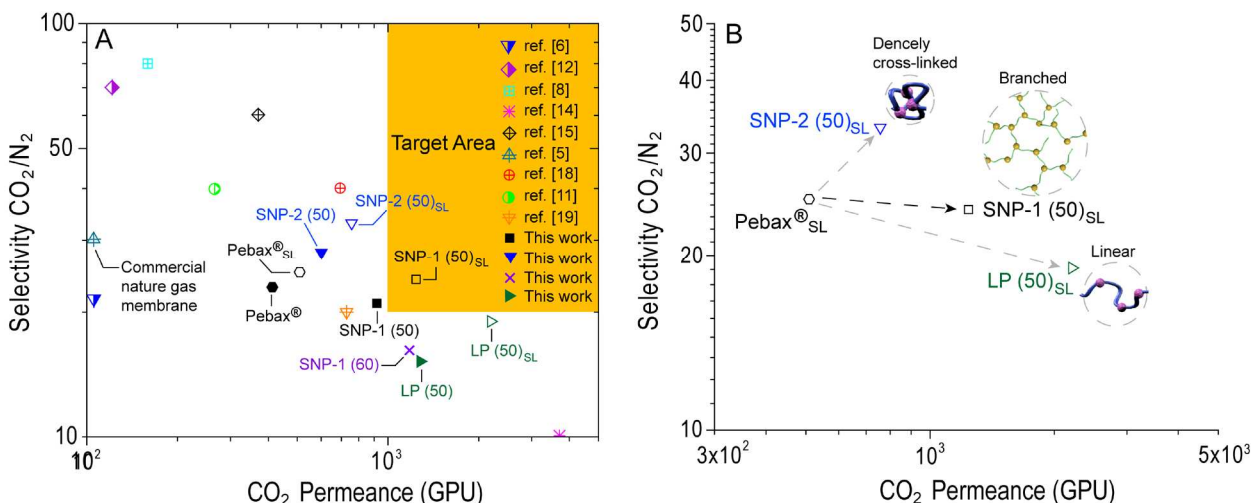


Fig. 4 (A) CO_2/N_2 selectivity versus CO_2 permeance plot comparing the performance of Pebax[®]/SNPs TFC membranes and their selective layers with commercial natural gas membranes and developmental membranes reported in the literature. The target area is proposed by Merkel *et al.*⁵ for post combustion capture of carbon dioxide. (B) The effect of SNPs morphologies on the TFC membrane performance.

Fig. 4A shows a trade-off plot of CO_2/N_2 selectivity versus CO_2 permeance. The target area for post combustion capture proposed by Merkel *et al.*⁵ is also included in the plot for comparison. Membranes having high CO_2 permeance (≥ 1000 GPU) with a modest selectivity (≥ 20) fall within this target performance area. As shown in Fig. 4A, the SNP-1 (50) TFC membrane and its selective layer SNP-1 (50)_{SL} possessed modest selectivity but higher CO_2 permeance (920 and 1,240 GPU, respectively) in comparison with most of the TFC membranes reported in the literature. The SNP-1 (50) membranes are approximately 9 times more permeable than conventional cellulose acetate membranes used for CO_2 removal from natural gas.⁵ In addition, the selective layer SNP-1 (50)_{SL} displayed excellent gas separation performance, falling within the CO_2 separation performance targeted area. The SNP-2 (50) TFC membrane and its selective layer SNP-2 (50)_{SL} exhibited modest CO_2 permeance improvements but higher CO_2/N_2 selectivity (28 and 33, respectively) in comparison with their SNP-1 counterparts.

Fig. 4B clearly indicates the effect of SNPs morphologies on their selective layers performance in this blend system. The incorporation of linear additive (LP of SNP-2) in Pebax[®] matrix induced a significant increase in CO_2 permeance but a decrease in CO_2/N_2 selectivity. By using highly branched SNP-1 as additives, the CO_2 permeance of SNP-1 (50)_{SL} was greatly increased while maintaining the CO_2/N_2 selectivity. The

addition of densely cross-linked SNP-2 to Pebax[®] matrix induced concurrent increase in CO₂ permeance and CO₂/N₂ selectivity.

Conclusion

In summary, we report a new approach to prepare Pebax[®] TFC membranes for CO₂ capture applications using amorphous SNPs with tunable morphologies. The highest CO₂ permeance with reasonable CO₂/N₂ selectivity was found for SNP-1 (50) TFC membrane with 50 wt. % SNP-1 mass fraction. The increased CO₂ permeance was due to the higher concentration of EG moieties and the increase in FFV within the selective layer. In addition, the SNP-1 (50)_{SL} fell within CO₂ separation performance targets for post combustion capture, with a CO₂ permeance of 1,280 GPU and a modest CO₂/N₂ selectivity of 24, which identifies them as a promising material for efficient CO₂ separation. Meanwhile, the SNP-2 (50) TFC membrane exhibited a concurrent increase in CO₂ permeability and CO₂/N₂ selectivity that is rarely observed and could possibly lead to the development of advanced gas separation membranes. This study also demonstrates the effects of SNPs morphologies on the TFC membrane performance. Our future work will focus on mixed gas permeation through these composite membranes.

Although the spin-coating technology used in this study is hard to scale-up, dip-coating technique may be employed to fabricate dual layer composite hollow fibre membranes. Additionally, a blade-casting approach could also be utilized to enable the large scale production of composite membranes, i.e. spiral wound membranes using these SNP additives for efficient gas separation application.

Acknowledgments

The authors acknowledge the funding provide by the Australian Government through the CRC program to support this research. The authors also acknowledge the Australian Research Council under the Future Fellowship (FT110100411, G.G.Q.) scheme for financial support of this work. Q.F. is the recipient of an Australian Research Council Super Science Fellowship (FS110200025). Q.F. and E.H.H.W. also wish to acknowledge

the receipt of 2013 and 2014 Early Career Researcher Grants from The University of Melbourne, respectively.

Notes and references

1. D. Aaron and C. Tsouris, *Separ. Sci. Technol.*, 2011, **40**, 321-348.
2. M. Zhao, A. I. Minett and A. T. Harris, *Energ. Environ. Sci.*, 2013, **6**, 25-40.
3. C. E. Powell and G. G. Qiao, *J. Membr. Sci.*, 2006, **279**, 1-49.
4. W. Yave, A. Car, J. Wind and K.-V. Peinemann, *Nanotechnology*, 2010, **21**, 395301-395307.
5. T. C. Merkel, H. Lin, X. Wei and R. Baker, *J. Membr. Sci.*, 2010, **359**, 126-139.
6. L. Liu, A. Chakma and X. Feng, *Ind. Eng. Chem. Res.*, 2005, **44**, 6874-6882.
7. L. Liu, A. Chakma and X. Feng, *J. Membr. Sci.*, 2004, **235**, 43-52.
8. A. Car, C. Stropnik, W. Yave and K.-V. Peinemann, *Sep. Sci. Technol.*, 2008, **62**, 110-117.
9. Q. Fu, A. Halim, J. Kim, J. M. P. Scofield, P. A. Gurr, S. E. Kentish and G. G. Qiao, *J. Mater. Chem. A*, 2013, **1**, 13769-13779.
10. H. Li, Z. Song, X. Zhang, Y. Huang, S. Li, Y. Mao, H. J. Ploehn, Y. Bao and M. Yu, *Science*, 2013, **342**, 95-98.
11. S. Zhao, Z. Wang, Z. Qiao, X. Wei, C. Zhang, J. Wang and S. Wang, *J. Mater. Chem. A*, 2013, **1**, 246-249.
12. S. Duan, F. A. Chowdhury, T. Kai, S. Kazama and Y. Fujiok, *Desalination*, 2008, **234**, 278-285.
13. S. Li, Z. Wang, X. Yu, J. Wang and S. Wang, *Adv. Mater.*, 2012, **24**, 3196-3200.
14. P. Li, H. Z. Chen and T.-S. Chung, *J. Membr. Sci.*, 2013, **434**, 18-25.
15. M. Sandru, S. H. Haukebo and M.-B. Hägg, *J. Membr. Sci.*, 2010, **346**, 172-186.
16. H. B. Park, C. H. Jung, Y. M. Lee, A. J. Hill, S. J. Pas, S. T. Mudie, E. V. Wagner, B. D. Freeman and D. J. Cookson, *Science*, 2007, **318**, 254-258.
17. N. Du, H. B. Park, G. P. Robertson, M. M. Dal-Cin, T. Visser, L. Scoles and M. D. Guiver, *Nat. Mater.*, 2011, **10**, 372-375.
18. W. Yave, A. Car, S. S. Funari, S. P. Nunes and K.-V. Peinemann, *Macromolecules*, 2010, **43**, 326-333.
19. A. Halim, Q. Fu, Q. Yong, P. A. Gurr, S. E. Kentish and G. G. Qiao, *J. Mater. Chem. A*, 2014, **2**, 4999-5009.
20. Q. Song, S. K. Nataraj, M. V. Roussenov, J. C. Tan, D. J. Hughes, W. Li, P. Bourgoïn, M. A. Alam, A. K. Cheetham, S. A. Al-Muhtaseb and E. Sivaniah, *Energ. Environ. Sci.*, 2012, **5**, 8359-8369.
21. Y. Li, S. Wang, H. Wu, J. Wang and Z. Jiang, *J. Mater. Chem.*, 2012, **22**, 19617-19620.
22. S. L. Liu, L. Shao, M. L. Chua, C. H. Lau, H. Wang and S. Quan, *Prog. Polym. Sci.*, 2013, **38**, 1089-1120.
23. J. H. Kim, S. Y. Ha and Y. M. Lee, *J. Membr. Sci.*, 2001, **190**, 179-193.
24. J. H. Kim and Y. M. Lee, *J. Membr. Sci.*, 2001, **193**, 209-225.
25. H. Lin and B. D. Freeman, *J. Membr. Sci.*, 2004, **239**, 105-117.
26. E. H. H. Wong, S. J. Lam, E. Nam and G. G. Qiao, *ACS Macro. Lett.*, 2014, **3**, 524-528.
27. J. Chiefari, Y. K. Chong, F. Ercole, J. Krstina, J. Jeffery, T. P. T. Le, R. T. A. Mayadunne, G. F. Meijs, C. L. Moad, G. Moad, E. Rizzardo and S. H. Thang, *Macromolecules*, 1998, **31**, 5559-5562.
28. J. M. Ren, Q. Fu, A. Blencowe and G. G. Qiao, *ACS Macro. Lett.*, 2012, **1**, 681-686.
29. A. Bos, I. G. M. PuEnt, M. Wessling and H. Strathmann, *J. Membr. Sci.*, 1999, **155**, 67-78.

TOC

Novel soft nanoparticles with tunable morphologies were incorporated into thin film composite membrane system for efficient CO₂ capture applications.

